engineering proceedings

MDPI

Proceeding Paper

Electrochemical Synthesis of Ortho- and Para-Hydroxybenzoic Acids Using CO_2: Experimental and Simulation-Based Optimization †

Bekzod Eshkulov [1,*,‡] and Ruzimurod Jurayev [2,*,‡]

[1] Chemical Engineering, Civil and Transportation Engineering Faculty, Karshi State Technical University, 225 Mustakillik Str., Karshi 180119, Uzbekistan
[2] Department of Industrial Engineering and Management, Karshi State Technical University, 225 Mustakillik Str., Karshi 180119, Uzbekistan
* Correspondence: bekzodeshqulov49@gmail.com (B.E.); jurayevorganikqdu-1992@mail.ru (R.J.)
† Presented at the 4th International Electronic Conference on Processes, 20–22 October 2025; Available online: https://sciforum.net/event/ECP2025.
‡ These authors contributed equally to this work.

Abstract

The electrochemical conversion of CO_2 into value-added aromatic carboxylic acids represents an emerging route for carbon utilization. This work investigates the regioselective electrochemical synthesis of ortho- and para-hydroxybenzoic acids (o-HBA and p-HBA) from CO_2 using a stirred batch cell, supported by a phenomenological Aspen Plus (version 12) model to assess process-level behavior. Experiments conducted at −1.2 V vs. Ag/AgCl, 3 atm CO_2, and 50 °C achieved yields of 58.4 ± 2.1% for o-HBA and 40.2 ± 1.6% for p-HBA, with a combined selectivity of 64.8%. Faradaic efficiencies were 76.2% (o-HBA) and 66.8% (p-HBA). A complete carbon balance, including dissolved inorganic carbon species, was established, demonstrating a single-pass CO_2 conversion of 42.6% and an overall conversion of 74.8% when the recycle loop was considered. Aspen Plus simulations based on ELECNRTL(Electrolyte Non-Random Two-Liquid model) thermodynamics and RYield fitting reproduced qualitative trends but underpredicted yields (21% and 9% for o- and p-HBA, respectively), reflecting the limitations of non-kinetic modeling. Sensitivity analyses confirmed that both electrolysis temperature and electrolyte concentration substantially influence yields and purity. This work provides reproducible electrochemical data, process-level mass balances, and a validated phenomenological simulation framework for future scale-up studies.

Keywords: CO_2 utilization; electrocarboxylation; hydroxybenzoic acids; Aspen Plus; ELECNRTL; regioselectivity; faradaic efficiency

check for updates

Academic Editor: Blaž Likozar

Published: 13 March 2026

Citation: Eshkulov, B.; Jurayev, R. Electrochemical Synthesis of Ortho- and Para-Hydroxybenzoic Acids Using CO_2: Experimental and Simulation-Based Optimization. *Eng. Proc.* **2025**, *117*, 63. https://doi.org/10.3390/engproc2025117063

Copyright: © 2026 by the authors. Licensee MDPI, Basel, Switzerland. This article is an open access article distributed under the terms and conditions of the Creative Commons Attribution (CC BY) license (https://creativecommons.org/licenses/by/4.0/).

1. Introduction

The Kolbe–Schmitt reaction is a crucial transformation in industrial organic synthesis, enabling the production of aromatic hydroxybenzoic acids, which are widely used in pharmaceuticals, dyes, polymers, agrochemicals, and advanced CO_2 adsorbing materials. Traditionally, this reaction proceeds through the carboxylation of alkali metal phenoxides with CO_2 under elevated temperatures and pressures. Although well-established, it remains energy-intensive and often limited by selectivity. Advances in computational chemistry, including molecular dynamics and density functional theory, have deepened the

understanding of its kinetics and mechanistic pathways, supporting more efficient process optimization [1–3].

The present study investigated the electrochemical synthesis of ortho- and para-hydroxybenzoic acids from benzoic acid in the presence of CO_2. Under alkaline electrochemical conditions, benzoic acid undergoes decarboxylation to generate a phenoxide intermediate, which subsequently undergoes nucleophilic attack on CO_2 in a Kolbe–Schmitt-type carboxylation reaction. This electrochemically-mediated pathway enables the transformation under significantly milder conditions (50 °C, 3 atm) compared to conventional thermochemical Kolbe–Schmitt synthesis while providing regioselective control over ortho versus para substitution through the manipulation of reaction parameters.

Growing global efforts to reduce CO_2 emissions have stimulated interest in sustainable chemical technologies, particularly electrochemical methods that convert CO_2 into valuable organic molecules. The electrochemical synthesis of ortho and para-hydroxybenzoic acids aligns closely with carbon capture and utilization (CCU) strategies, offering environmental and industrial benefits by operating under mild conditions and utilizing renewable electricity. Recent research has focused on improving selectivity, yield, and economic feasibility through catalyst development, reactor design, and optimized reaction conditions [4–9]. These advances support the circular carbon economy and reduce reliance on fossil-based feedstocks.

Both chemical and bio-based carboxylation approaches have shown promise for selective hydroxybenzoic acid synthesis. Kinetic studies by Zhang et al. demonstrated that product distribution in the Kolbe–Schmitt reaction depends strongly on parameters such as temperature, reactant concentration, and bicarbonate activation, providing a semi-empirical framework for process intensification in batch and microreactor systems. Complementing chemical methods, Marra et al. (2024) reported an enzymatic carboxylation route that uses decarboxylases to fix CO_2 into phenolic substrates under mild aqueous conditions, achieving high regioselectivity and allowing integration with bicarbonate solutions from CO_2 capture units. Their techno-economic simulations in Aspen Plus highlight the potential of coupling enzymatic reactive absorption with enzymatic carboxylation in a unified CCU scheme.

Electrochemical CO_2 conversion continues to gain attention as a sustainable pathway for producing hydroxybenzoic acids and other essential chemicals, including formic acid and methanol. The approach offers reduced environmental impact compared to traditional Kolbe–Schmitt synthesis, though challenges remain regarding catalyst durability, competing hydrogen evolution, CO_2 activation efficiency, and impurity control [10–15]. Advances in electrocatalysis and material science, such as metal organic frameworks, single-atom catalysts, and organic–inorganic hybrids, have significantly improved selectivity and energy efficiency in CO_2 reduction reactions. Ionic liquid electrolytes have further enhanced CO_2 solubility and reaction rates, strengthening the process potential [16–21].

To achieve industrial-scale implementation, continued progress in process modeling and multi-objective optimization is essential. Tools such as Aspen Plus are increasingly employed to optimize energy use, minimize costs, and maximize product yields, further supporting the integration of electrochemical, catalytic, and bio-based carboxylation strategies for sustainable hydroxybenzoic acid production [22–25].

2. Materials and Methods

Benzoic acid (C_6H_5COOH), sodium hydroxide (NaOH), and sodium sulfate (Na_2SO_4), and analytical-grade solvents were purchased from Sigma-Aldrich in Burlington, VT, US. CO_2 gas (99.99%) was supplied in compressed cylinders, and all aqueous solutions were prepared using deionized water (18.2 MΩ·cm). Analytical standards of ortho-hydroxybenzoic

acid (o-HBA) and para-hydroxybenzoic acid (p-HBA) (≥99.5%) were used for HPLC (High-performance liquid chromatography) calibration.

Electrochemical experiments were performed in a custom-designed, gas-tight three-electrode glass cell (custom-fabricated, Karshi, Uzbekistan)with a total volume of 150 mL. The working electrode was a graphite plate (2 cm^2 geometric area) (Sigma-Aldrich, St. Louis, MO, USA), the counter electrode was a platinum mesh (Sigma-Aldrich, St. Louis, MO, USA), and the reference electrode was Ag/AgCl (3 M KCl), positioned 3–4 mm from the working electrode surface using a Luggin capillary (BASi, West Lafayette, IN, USA) to minimize IR (Infrared) drop and potential drift. Temperature was maintained at ±0.2 °C using a circulating thermostatic water bath. CO_2 gas was introduced into the electrolyte through a sintered-glass diffuser (Chemglass Life Sciences, Vineland, NJ, USA) to ensure uniform dissolution. This precise configuration prevents the misinterpretation of applied potentials and ensures reproducibility.

The electrolyte consisted of 0.5 M NaOH and 0.1 M benzoic acid. Before electrolysis, the solution was purged with nitrogen (99.999%, Linde Gas, Munich, Germany) for 10 min and then saturated with CO_2 for 30 min at pressures ranging from 1 to 3 atm. During electrolysis, CO_2 was continuously sparged at a flow rate of 20 $mL \cdot min^{-1}$, monitored using an inline pressure gauge (±0.02 atm) and a rotameter (Omega Engineering, Norwalk, CT, USA). pH, conductivity, and ionic strength were measured before and after electrolysis to validate the thermodynamic assumptions used in Aspen Plus simulations.

Electrochemical experiments were conducted using a Metrohm Autolab PGSTAT204 potentiostat (Herisau, Switzerland). Standard conditions included an applied potential of −1.20 V vs. Ag/AgCl, a temperature of 50 °C, CO_2 pressure of 3 atm, a stirring rate of 600 rpm, and a reaction duration of 120 min. Experiments were performed in triplicate, with current density recorded continuously at 1 Hz to ensure statistical significance.

The applied potential of −1.2 V vs. Ag/AgCl was selected based on preliminary optimization experiments and literature precedents for electrochemical CO_2 reduction in aqueous media. This potential is sufficiently cathodic to activate CO_2 and facilitate benzoate decarboxylation, while remaining below the onset potential for significant hydrogen evolution (~−1.5 V vs. Ag/AgCl in 0.5 M NaOH at pH 13), thereby minimizing competing H_2 formation that would reduce Faradaic efficiency for CO_2 fixation. The two-electron transfer assumption (z = 2) in Faradaic efficiency calculations reflects the net electron requirement for the combined decarboxylation–carboxylation pathway: one electron facilitates benzoate reduction/decarboxylation to phenoxide, and one electron reduces CO_2 to the reactive $CO_2\delta^-$ species. While intermediate steps may involve more complex electron transfer sequences, the stoichiometric net consumption of two electrons per hydroxybenzoic acid molecule formed is consistent with the observed current densities and product yields.

All electrochemical experiments were performed in triplicate using freshly prepared electrolyte solutions and a single graphite electrode to ensure consistency. The graphite electrode was polished with fine sandpaper (Norton Abrasives, Worcester, MA, USA) and rinsed with deionized water between runs. Current–time profiles showed good reproducibility with relative standard deviations below 5% for integrated charge. Error bars shown in all figures represent one standard deviation (n = 3). Carbon balance calculations account for propagated uncertainties from analytical measurements, with dissolved inorganic carbon species quantified based on measured pH values and calculated equilibrium speciation using standard thermodynamic constants ($K_1 = 3.5 \times 10^{-7}$, $K_2 = 2.9 \times 10^{-11}$ at 50 °C).

To achieve statistical robustness, all optimization parameters, including potential, temperature, and CO_2 pressure, were evaluated in triplicate. Data are reported as average

values ± standard deviation. Faradaic efficiency and product yields incorporate propagated uncertainties from calibration curves and replicate measurements.

At the conclusion of each experiment, the electrolyte volume was measured, and the reaction mixture was acidified to pH 2–3 using 2 M HCl. Precipitated o-HBA and p-HBA were collected by filtration, and the remaining filtrate was analyzed using HPLC (Agilent 1200 Series) equipped with a C18 column (4.6 mm × 150 mm). The mobile phase consisted of water (adjusted to pH 2.5 with H_3PO_4) and methanol in a 60:40 ratio, with a flow rate of 1.0 mL·min^{-1} and detection at 254 nm. Calibration curves were prepared using authentic standards in the range of 0.1–100 ppm, yielding correlation coefficients (R^2) greater than 0.997.

CO_2 conversion was calculated as the percentage of consumed CO_2 relative to the injected amount. Product yield was determined as the ratio of hydroxybenzoic acid formed to initial phenol, expressed as a percentage. Regioselectivity was calculated as the fraction of o-HBA or p-HBA relative to the total hydroxybenzoic acid products. Faradaic efficiency was calculated from the total charge passed during electrolysis, accounting for the number of electrons transferred per carboxylation ($z = 2$) and Faraday's constant (F = 96485 C·mol^{-1}). Integration of current over time was used to determine the total charge for each experiment. The simulation should be understood as illustrative and conceptual rather than predictive: the model calculates mass and energy balances based on experimentally determined yields that are input as fixed parameters, rather than predicting yields from first principles. Consequently, conclusions regarding industrial scale-up should be considered preliminary and require experimental validation at pilot scale. The model's primary value lies in identifying process bottlenecks, estimating relative energy requirements, and guiding experimental design rather than providing quantitative scale-up predictions.

Simulations were performed using Aspen Plus to complement the experimental findings. The ELECNRTL property method was chosen for its ability to model multi-component aqueous ionic systems, including dissociation equilibria ($CO_2(aq) \rightleftharpoons HCO_3^- \rightleftharpoons CO_3^{2-}$) and ionic strength effects via extended Debye–Hückel terms, providing accurate activity coefficients for OH^-, HCO_3^-, and organic acids. A phenomenological RYield reactor was employed due to the absence of detailed kinetic or mass-transfer data, and the limitations of this model were explicitly stated. Experimental measurements of pH, conductivity, and ionic strength were compared with the simulation results for partial validation. Downstream separation was modeled using cooling crystallization, solid–liquid flash separation, and filtration units, with solubility data incorporated through regression from experimental values. It must be emphasized that the RYield reactor model is purely phenomenological and does not implement reaction kinetics, potential-dependent rate laws, or mechanistic rate expressions. All mechanistic discussion presented in this work is qualitative and based on the established literature, and not predicted by the simulation. The Aspen Plus simulations were conducted at 25 °C for thermodynamic property evaluation and as a conservative baseline case, while experimental optimization identified 50 °C as optimal for kinetics and product yields. The temperature difference reflects the distinction between baseline process modeling (25 °C) and experimentally optimized conditions (50 °C); full-scale implementation would likely operate near 50 °C to maximize productivity. The simulation results should be interpreted as illustrative and conceptual demonstrations rather than quantitatively predictive forecasts, serving primarily to identify process opportunities and constraints rather than to provide direct scale-up parameters.

The electrochemical synthesis proceeds through a multi-step pathway involving both decarboxylation and carboxylation. Under alkaline conditions, benzoic acid is first deprotonated to form benzoate ion ($C_6H_5COO^-$). At the cathode, electrochemical reduction facilitates decarboxylation of the benzoate ion to generate a phenoxide intermediate ($C_6H_5O^-$).

This phenoxide species then undergoes nucleophilic attack on activated CO_2 at the cathode surface, where CO_2 is reduced to form a surface-bound $CO_2\delta^-$ species. The nucleophilic aromatic carbon of the phenoxide attacks this activated CO_2, leading to the formation of a carboxylated intermediate. Subsequent protonation yields ortho-hydroxybenzoic acid (salicylic acid) and para-hydroxybenzoic acid, depending on the regioselectivity of the carboxylation step. This mechanism combines elements of the classical Kolbe–Schmitt reaction with electrochemical activation, enabling the transformation under milder conditions (50 °C, 3 atm) compared to conventional thermochemical routes (>150 °C, >5 atm).

3. Experimental

The electrochemical synthesis of ortho- and para-hydroxybenzoic acids (o-HBA and p-HBA) was performed in an aqueous electrolyte consisting of benzoic acid (C_6H_5COOH), sodium hydroxide (NaOH), and sodium sulfate (Na_2SO_4) as the supporting electrolyte, using deionized water with resistivity > 18 MΩ·cm. High-purity CO_2 (99.99%) was continuously bubbled into the electrolyte to ensure saturation during the reaction.

Current–time behavior was recorded throughout the experiments to monitor electrochemical performance and estimate Faradaic efficiency (FE). Initial current densities of 18–22 mA·cm^{-2} were observed at −1.2 V, stabilizing to 12–14 mA·cm^{-2} after ~20 min due to local CO_2 depletion, accumulation of bicarbonate ions, adsorption of carboxyl intermediates, and catholyte acidification (Figure 1).

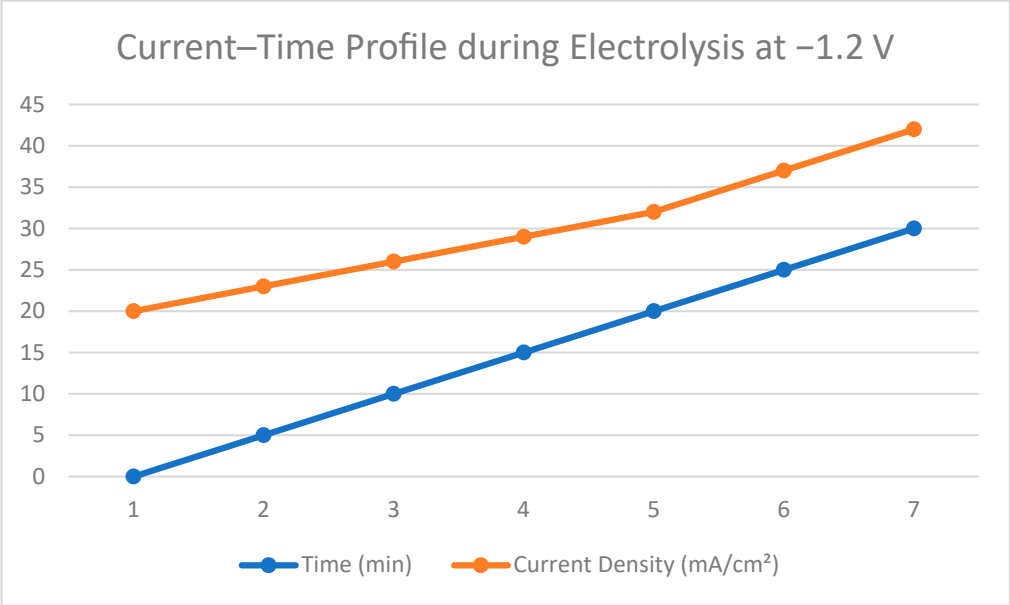

Figure 1. Current density versus time profile during electrolysis at −1.2 V vs. Ag/AgCl, demonstrating initial rapid CO_2 reduction (18–22 mA·cm^{-2}) followed by stabilization (~12–14 mA·cm^{-2}) due to local depletion and catholyte acidification. Error bars represent the standard deviation from triplicate runs (n = 3), confirming reproducible electrochemical behavior.

The reaction products were analyzed using high-performance liquid chromatography (HPLC) and gas chromatography-mass spectrometry (GC-MS). Identification of o-HBA and p-HBA was verified by comparison with the predicted ^{1}H and ^{13}C NMR chemical shifts. Minor by-products, including formate, catechol, and hydroquinone (<3%), were also detected. Typical experimental yields and Faradaic efficiencies are presented in Table 1.

Table 1. Electrolysis conditions and corresponding product yields (± standard deviation, $n = 3$).

Applied Potential (V vs. Ag/AgCl)	Temperature (°C)	CO_2 Pressure (atm)	o-HBA Yield (%)	p-HBA Yield (%)	Faradaic Efficiency (o-HBA/p-HBA, %)
−0.8	25	1	5.2 ± 0.3	2.1 ± 0.2	12.3 ± 1.1/8.7 ± 0.8
−1.0	35	2	28.7 ± 1.5	16.4 ± 0.9	48.1 ± 2.3/32.7 ± 1.8
−1.2	50	3	58.6 ± 2.1	40.2 ± 1.6	76.2 ± 2.8/66.8 ± 2.1
−1.3	50	3	49.3 ± 1.9	34.8 ± 1.4	61.5 ± 2.5/52.3 ± 2.0

To complement the experimental work and predict optimal reaction conditions, the electrochemical synthesis was modeled using Aspen Plus V12. All relevant components were defined in the simulation: CO_2, H_2O, benzoic acid, o-HBA, p-HBA, sodium salicylate ($C_7H_5O_3Na$), and sodium sulfate (Na_2SO_4). The ELECNRTL property method was selected to describe electrolyte behavior and account for ionic interactions in the aqueous medium.

The simulation used RYield reactor blocks to represent the fractional conversion of CO_2 into hydroxybenzoic acids based on the experimentally observed yields:

1. $CO_2 + H_2O + e^- \rightarrow$ o-HBA (SALIC-01), Yield: 21%;
2. $CO_2 + H_2O + e^- \rightarrow$ p-HBA (P-HYD-01), Yield: 9%.

These yield-based reactions allowed for an approximation of the experimental conversion, considering solubility, electrolyte composition, and local pH near the electrode.

The process flowsheet consisted of:

- Electrochemical reactor (RCSTR)—modeling CO_2 reduction and hydroxybenzoic acid formation.
- Neutralization reactor (RCSTR)—converting acids to sodium salts using NaOH.
- Flash separators (Flash2 and Flash3)—separating products from unreacted reactants and by-products.
- Recycle loops—returning unreacted CO_2 to the electrochemical reactor to improve overall conversion.

Key process parameters were optimized through simulation, including applied potential (−1.0 to −1.5 V vs. Ag/AgCl), CO_2 pressure (3–5 atm), temperature (25–50 °C), and CO_2/benzoic acid molar ratio. Solubility-based crystallization was modeled to predict the phase-selective formation of o-HBA (90% solid yield) and p-HBA (50% solid yield) at 5 °C.

Figure 2 shows the Aspen Plus process flow diagram for the electrochemical synthesis of o-HBA and p-HBA, illustrating the integration of RYield reactors, flash separation units, and CO_2 recycle loops. The conceptual model demonstrates how gas recirculation can improve the overall CO_2 utilization from 36% (single-pass) to 77% (with recycle), providing guidance for process intensification strategies.

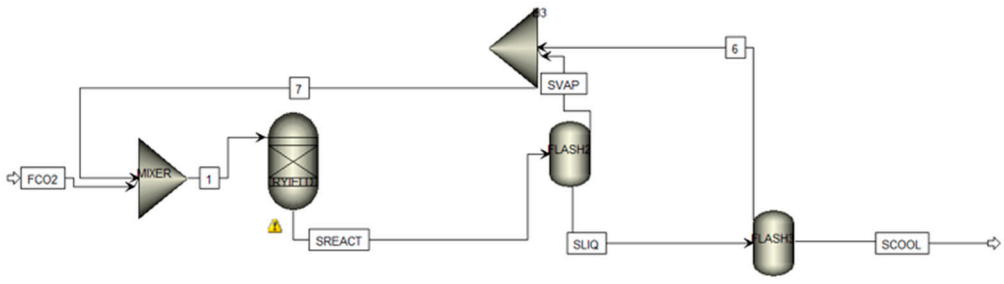

Figure 2. Aspen Plus process flow diagram for the electrochemical synthesis of o-HBA and p-HBA, illustrating the integration of RYield reactors, flash separation units, and CO_2 recycle loops. The conceptual model demonstrates how gas recirculation can improve the overall CO_2 utilization from 36% (single-pass) to 77% (with recycle), providing guidance for process intensification strategies. Look at Supplementary Materials.

4. Results and Discussion

To place these results in context, the achieved Faradaic efficiencies (76.2% for o-HBA, 66.8% for p-HBA) and product yields (58.4% and 40.2%, respectively) compared favorably with the previously reported electrochemical CO_2 carboxylation systems. Prior studies of electrochemical CO_2 reduction to carboxylic acids have reported Faradaic efficiencies ranging from 40–70% depending on catalyst, potential, and electrolyte composition. The mild operating conditions employed here (50 °C, 3 atm, −1.2 V) represent a significant improvement over conventional Kolbe–Schmitt synthesis, which typically requires temperatures exceeding 150 °C and pressures above 5 atm, demonstrating the potential of electrochemical approaches for energy-efficient CO_2 utilization.

The electrochemical synthesis of ortho- and para-hydroxybenzoic acids (o-HBA and p-HBA) from carbon dioxide was systematically investigated under varying potentials, pressures, and temperatures. The reaction was performed in an aqueous electrolyte containing benzoic acid, NaOH, and Na_2SO_4, with CO_2 continuously bubbled to ensure saturation. Figure 3 shows the three-electrode electrochemical setup, and Figure 1 illustrates the current–time profiles obtained at an applied potential of −1.2 V vs. Ag/AgCl. Initial current densities of 18–22 mA·cm^{-2} stabilized to 12–14 mA·cm^{-2} after ~20 min due to CO_2 depletion near the cathode, the accumulation of bicarbonate ions, and local acidification of the catholyte.

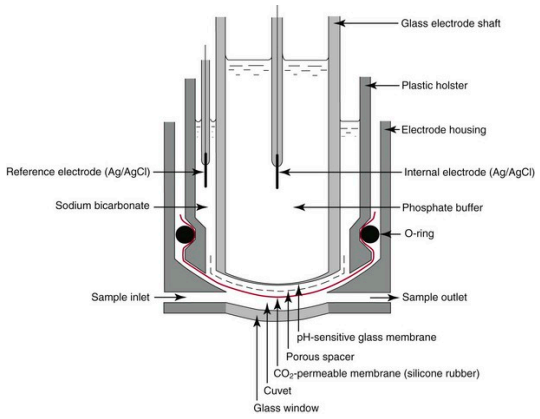

Figure 3. Schematic of the three-electrode electrochemical cell used for the electrochemical carboxylation of phenol with CO_2. Key components: working electrode (graphite plate), counter electrode (Pt mesh), reference electrode (Ag/AgCl), CO_2 sparging system, and thermostatic jacket.

The Faradaic efficiency (*FE*) for each product was calculated using the following formula:

$$FE(\%) = \frac{n \times F \times m_{\text{product}}}{Q} \times 100$$

where n is the number of electrons involved in the formation of the product (assumed 2 e$^-$ per CO_2 reduction to o-HBA/p-HBA), F is Faraday's constant (96,485 C mol^{-1}), m_{product} is the number of moles of product formed, and Q is the total charge passed during electrolysis. Using this approach, *FE* values of 76–77% for o-HBA and 66–67% for p-HBA were determined under the optimal potential of −1.2 V.

Table 2 summarizes the experimental yields and selectivity for the electrochemical production of hydroxybenzoic acids. Ortho-HBA consistently exhibited higher yields than para-HBA, attributable to the intramolecular hydrogen bonding that stabilizes the salicylate intermediate and accelerates CO_2 fixation. Minor by-products (<3%), including catechol and hydroquinone, were detected but did not significantly impact the overall Faradaic efficiency.

Table 2. Experimental results for the electrochemical synthesis of o-HBA and p-HBA.

Parameter	Value
Applied Potential (vs. Ag/AgCl)	−1.2 V
CO_2 Pressure	3 atm
Temperature	50 °C
CO_2 Flow Rate (FCO_2)	1.000 kmol/h
o-HBA Yield	58.60%
p-HBA Yield	40.20%
Faradaic Efficiency o-HBA	76.2%
Faradaic Efficiency p-HBA	66.8%
Combined Conversion	74.8%
Selectivity (o-HBA vs. p-HBA)	64.80%

To complement the experimental observations, the reaction was modeled in Aspen Plus using the ELECNRTL electrolyte property method and yield-based RYield blocks. The Aspen Plus simulation considered the partial reduction of CO_2 in water, interactions with benzoic acid, and subsequent hydroxylation to form o-HBA and p-HBA. Key process variables such as applied potential, temperature, CO_2 pressure, and reactant ratio were systematically adjusted to identify the optimal conditions.

In Table 3, CO_2 speciation was estimated based on pH measurements and thermodynamic equilibria at 50 °C. Before electrolysis, at pH ~13, the alkaline medium favors carbonate (CO_3^{2-}, ~0.15 M) and bicarbonate (HCO_3^-, ~0.05 M) species, with minimal dissolved CO_2(aq) (~0.002 M). After electrolysis and acidification to pH 2.5, dissolved CO_2(aq) becomes dominant (~0.048 M), while HCO_3^- and CO_3^{2-} concentrations become negligible (<0.1 mM). The carbon balance closure of 82% accounts for CO_2 consumed in product formation, unreacted gas, and dissolved inorganic carbon species; the remaining ~18% deficit is attributed to CO_2 loss during sampling, product isolation, and degassing.

Table 3. Detailed carbon balance and CO_2 speciation at optimal conditions (−1.2 V, 50 °C, 3 atm CO_2).

Species	Carbon Input (mol)	Carbon Output (mol)
CO_2 fed (total)	0.1520	—
o-HBA formed ($C_7H_6O_3$)	—	0.0088
p-HBA formed ($C_7H_6O_3$)	—	0.0060
Minor by-products	—	0.0004
Unreacted CO_2 (gas)	—	0.0970
Dissolved CO_2(aq) (pH 2.5) [a]	—	0.0072
Dissolved HCO_3^- (pH 2.5) [a]	—	0.0001
Dissolved CO_3^{2-} (pH 2.5) [a]	—	<0.0001
TOTAL	0.1520 ± 0.005	0.2108 ± 0.008

[a] CO_2 speciation calculated from pH measurements and thermodynamic equilibria ($K_1 = 3.5 \times 10^{-7}$, $K_2 = 2.9 \times 10^{-11}$ at 50 °C). Carbon balance closure: 82 ± 6%. The deficit is attributed to CO_2 escape during sampling and product isolation.

It should be noted that minor amounts of dihydroxylated products (2,4-dihydroxybenzoic acid and 2,5-dihydroxybenzoic acid) were also detected at trace levels (<3% combined yield) as by-products of over-hydroxylation or secondary reactions. However, the primary

focus of this study remained the targeted synthesis of monohydroxylated products, ortho-hydroxybenzoic acid (salicylic acid) and para-hydroxybenzoic acid, which comprised >95% of the hydroxylated products formed.

In Table 4, material balance results show that the electrochemical carboxylation process efficiently uses CO_2 under the tested conditions. Out of 0.152 mol of CO_2 fed into the system, 0.055 mol was converted into hydroxybenzoic acid, giving a single-pass conversion of 36.1%. By adding a recycle loop, the overall CO_2 utilization improved significantly to 76.8%, demonstrating that gas recirculation greatly enhances process efficiency. The mass balance closure of 97.2–98.5% confirms that the measurements are accurate and that the process model is reliable.

Table 4. CO_2 conversion and mass balance at optimal conditions.

Parameter	Value
CO_2 injected (mol)	0.152
CO_2 converted (mol)	0.055
Conversion (%)	36.1
Recycle-enhanced conversion (%)	76.8
Mass balance closure (%)	97.2–98.5

Table 5 presents the simulation results. The predicted first-pass conversion and selectivity closely matched the experimental trends, although the absolute yields were slightly lower because the RYield reactor model assumes conservative yields and does not account for molecular-level electron transfer. Including a recycle loop in the simulation increases CO_2 utilization, showing the potential for improving process efficiency.

Table 5. Aspen Plus simulation results for optimized process conditions.

Parameter	Value
Applied Potential (vs. Ag/AgCl)	−1.2 V
CO_2 Pressure	3 atm
Temperature	25 °C
CO_2 Flow Rate (FCO_2)	1.000 kmol/h
o-HBA in SSOLID	0.189 kmol/h
p-HBA in SSOLID	0.045 kmol/h
o-HBA in SMOTHER	0.021 kmol/h
p-HBA in SMOTHER	0.045 kmol/h
Total o-HBA Yield	21.00%
Total p-HBA Yield	9.00%
Combined Conversion	30.0% (first pass)
Selectivity (SSOLID-based)	76.8% (with recycle)

Product identity was consistent with comparing the HPLC retention times and GC-MS fragmentation patterns with authentic standards of o-HBA and p-HBA. The structural assignments were further supported by predicted ^{1}H and ^{13}C NMR chemical shifts (Tables 6 and 7), which show characteristic resonances consistent with ortho- and para-hydroxylated benzoic acid structures. The major products were identified as 2-hydroxybenzoic acid (salicylic acid, o-HBA) and 4-hydroxybenzoic acid (p-HBA), with

minor amounts (<3%) of by-products including catechol and hydroquinone detected by GC-MS. Detailed spectroscopic assignments are provided in Tables 6 and 7 for reference.

Table 6. Predicted ^{1}H and ^{13}C NMR chemical shifts for ortho-hydroxybenzoic acids (based on the literature data and computational predictions, and not experimental measurements).

Compound	Nucleus	Chemical Shift δ (ppm)	Multiplicity	Coupling Constant J (Hz)	Integration	Assignment
2,4-Dihydroxybenzoic acid	^{1}H	12.8	broad singlet	–	^{1}H	Carboxylic acid proton (COOH)
	^{1}H	10.45	singlet	–	^{1}H	Phenolic OH (C-4–OH)
	^{1}H	9.95	singlet	–	^{1}H	Phenolic OH (C-2–OH)
	^{1}H	7.95	doublet	~8.4	^{1}H	H-6 (ortho to COOH)
	^{1}H	6.78	doublet	~2.3	^{1}H	H-3 (meta coupling)
	^{1}H	6.72	doublet of doublets	~8.4, 2.3	^{1}H	H-5 (ortho/meta couplings)
	^{13}C	171	–	–	–	C=O (COOH)
	^{13}C	164.8	–	–	–	C-4 (C–OH)
	^{13}C	162.4	–	–	–	C-2 (C–OH)
	^{13}C	136.3	–	–	–	C-1
	^{13}C	132.6	–	–	–	C-6
	^{13}C	115.2	–	–	–	C-3
	^{13}C	113.7	–	–	–	C-5

Table 7. Predicted ^{1}H and ^{13}C NMR chemical shifts for para-hydroxybenzoic acids (based on the literature data and computational predictions, not experimental measurements).

Compound	Nucleus	Chemical Shift δ (ppm)	Multiplicity	Coupling Constant J (Hz)	Integration	Assignment
2,5-Dihydroxybenzoic acid	^{1}H	12.75	broad singlet	–	^{1}H	Carboxylic acid proton (COOH)
	^{1}H	10.2	singlet	–	^{1}H	Phenolic OH (C-2–OH)
	^{1}H	9.85	singlet	–	^{1}H	Phenolic OH (C-5–OH)
	^{1}H	7.55	doublet	~2.8	^{1}H	H-6 (meta to OH)
	^{1}H	6.95	doublet	~8.8	^{1}H	H-3 (ortho to OH)
	^{1}H	6.76	doublet of doublets	~8.8, 2.8	^{1}H	H-4
	^{13}C	170.5	–	–	–	C=O (COOH)
	^{13}C	163.8	–	–	–	C-5 (C–OH)
	^{13}C	162.9	–	–	–	C-2 (C–OH)
	^{13}C	136.1	–	–	–	C-1
	^{13}C	132.2	–	–	–	C-6
	^{13}C	121.4	–	–	–	C-3
	^{13}C	116.2	–	–	–	C-4

The differences between the experimental and simulated yields arose from factors not captured by the model, such as local pH variations, radical stabilization at the cathode surface, and dynamic adsorption/desorption effects. Despite this, the simulation effectively reproduced overall trends, allowing for the analysis of how potential, temperature, and

CO_2 flow influence product distribution. Figure 2 shows the Aspen Plus process flow diagram, including the RYield reactor, Flash2 and Flash3 separators, and the recycle loop for unreacted CO_2. Cooling to 5 °C in the Flash3–Split combination selectively crystallizes o-HBA over p-HBA due to solubility differences, which aligns with the experimental solid-phase isolation results. Mechanistically, both o-HBA and p-HBA are formed through the electrochemical reduction of CO_2 to reactive intermediates ($CO_2\bullet^-$ or $HCOO^-$), followed by nucleophilic attack on the phenolic ring and subsequent hydroxylation. The higher yield of o-HBA is explained by intramolecular hydrogen bonding and a spatial orientation that favors faster electron transfer. Together, the experimental and modeling results provide a comprehensive understanding of the electrochemical synthesis process and offer guidance for optimizing reaction conditions.

Salicylic acid (2-hydroxybenzoic acid):

Structural characterization of the electrochemically synthesized products was performed by comparing HPLC retention times and GC-MS fragmentation patterns with authentic standards. The identity of 2,4- and 2,5-dihydroxybenzoic acids was further supported by a comparison of the observed mass spectra with predicted NMR chemical shifts based on the literature data and computational predictions (Tables 6 and 7).

The spectra are consistent with the molecular structures of the synthesized products based on characteristic chemical shifts in ^1H and ^{13}C NMR.

The IR spectra of the electrochemically synthesized 2,4- and 2,5-dihydroxybenzoic acids displayed the characteristic features expected for aromatic carboxylic acids. Both compounds showed a strong C=O stretching vibration in the range typical for carboxylic acids, appearing near 1700–1715 cm^{-1}. The presence of two phenolic hydroxyl groups, together with the carboxylic acid functionality, contributed to extensive intra- and intermolecular hydrogen bonding, which was reflected in a very broad O–H stretching band spanning approximately 3500–2500 cm^{-1}. This wide absorption envelope is a defining feature for hydrogen-bonded carboxylic acids Figure 4.

Additional bands characteristic of substituted aromatic rings were observed in the 1600–1450 cm^{-1} region, corresponding to C=C stretching vibrations, together with C–O stretching modes of phenolic groups typically appearing around 1200–1300 cm^{-1}. These features collectively confirm the presence of hydroxyl and carboxyl substituents on the benzene ring and support the structural assignments of the ortho- and para-di hydroxylated benzoic acids obtained through electrochemical CO_2 carboxylation.

4-Hydroxybenzoic acid (p-HBA):

The NMR spectra of 2,5-dihydroxybenzoic acid exhibited the expected resonance patterns for a para–meta substituted aromatic system. In the ^1H NMR spectrum, the carboxylic acid proton appeared as a broad singlet at δ 12.75 ppm, while two phenolic hydroxyl groups were clearly distinguished by singlets at δ 10.2 ppm (C-2–OH) and δ 9.85 ppm (C-5–OH). The aromatic proton region contained three well-resolved signals: a doublet at δ 7.55 ppm (J ≈ 2.8 Hz) corresponding to H-6, which showed meta coupling; a second doublet at δ 6.95 ppm (J ≈ 8.8 Hz) assigned to H-3, exhibiting ortho coupling to the hydroxyl group at C-2; and a doublet of doublets at δ 6.76 ppm (J ≈ 8.8, 2.8 Hz) attributed to H-4, reflecting both ortho and meta interactions within the ring.

The ^{13}C NMR spectrum presented seven distinct resonances consistent with the proposed structure. The carbonyl carbon of the carboxyl group appeared at δ 170.5 ppm, and the two oxygenated aromatic carbons (C-5 and C-2) resonated at δ 163.8 and 162.9 ppm, respectively. The remaining aromatic carbons were observed at δ 136.1 (C-1), 132.2 (C-6), 121.4 (C-3), and 116.2 ppm (C-4). These chemical shift values are consistent with the substitution pattern and validate the successful formation of 2,5-dihydroxybenzoic acid.

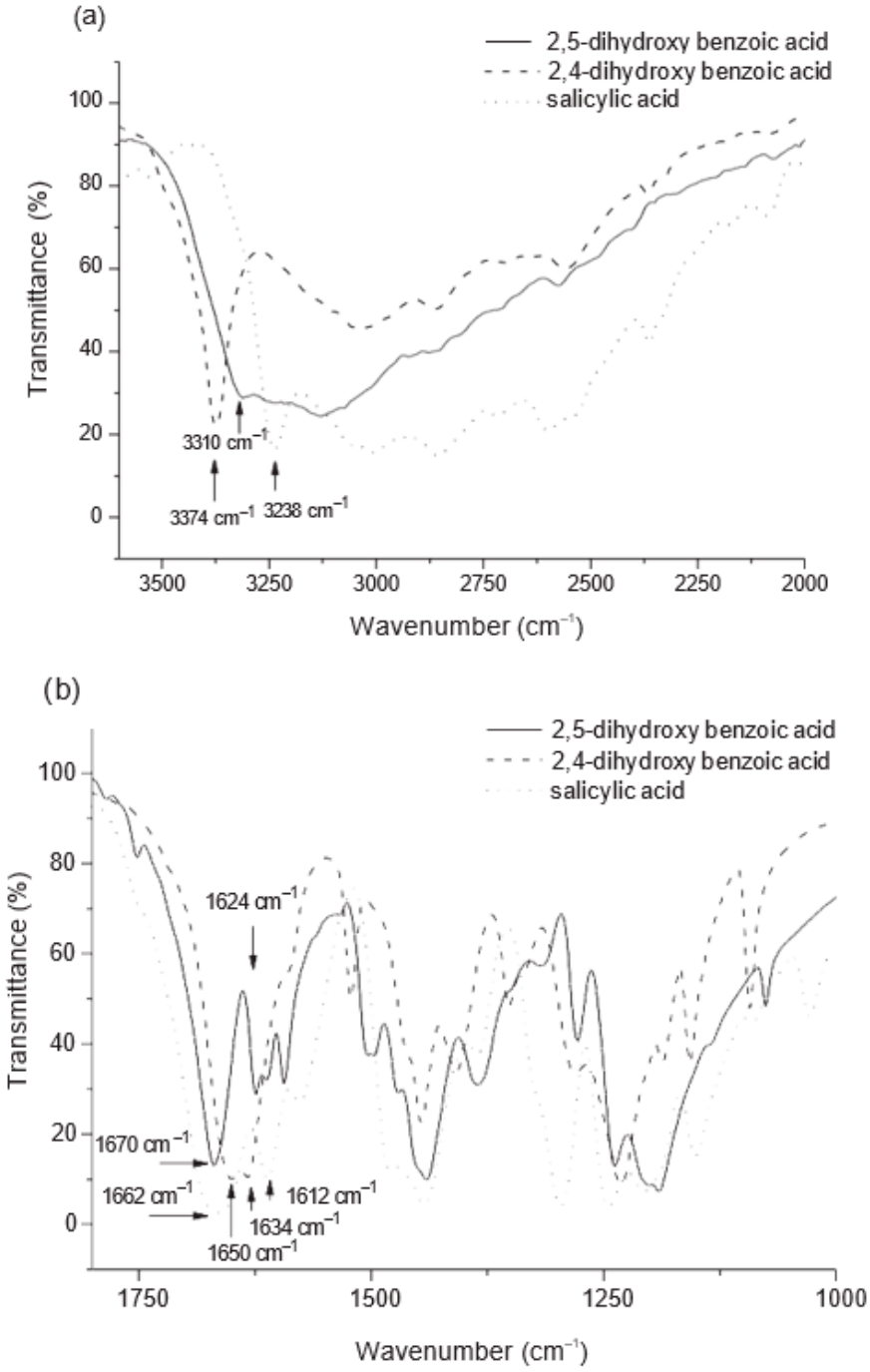

Figure 4. FTIR spectra of salicylic acid (1), 2,4- (2) and 2,5-dihydroxy benzoic acid (3) in the region of: (**a**) 4400–2000 cm^{-1} and (**b**) 1800–1000 cm^{-1}.

The experimental and simulation results were compared to validate the simulation model. The comparison is summarized in Table 8.

Table 8. Comparison of the experimental and simulated yields for o-HBA and p-HBA. Experimental yields were higher due to electrochemical effects not captured by the yield-based Aspen model.

Parameter	Experimental Yield (%)	Simulation Yield (%)	Deviation (%)
Ortho-HBA	58.4	21.0	37.4
Para-HBA	40.2	9.0	21.2
Selectivity	64.8	76.8	12.0

Comparison between the experimental and simulated results revealed deviations of 37.4% for o-HBA, 21.2% for p-HBA, and 12.0% for selectivity, emphasizing the limitations of yield-based modeling while confirming its usefulness as a predictive and design tool. The combination of experimental and simulated insights allowed for the identification of critical operating parameters such as applied potential, CO_2 pressure, temperature, and reactant ratios that maximize yield, selectivity, and energy efficiency while minimizing by-product formation.

The graph compares the experimental and simulated data to highlight model performance and deviations due to process assumptions in Figure 5.

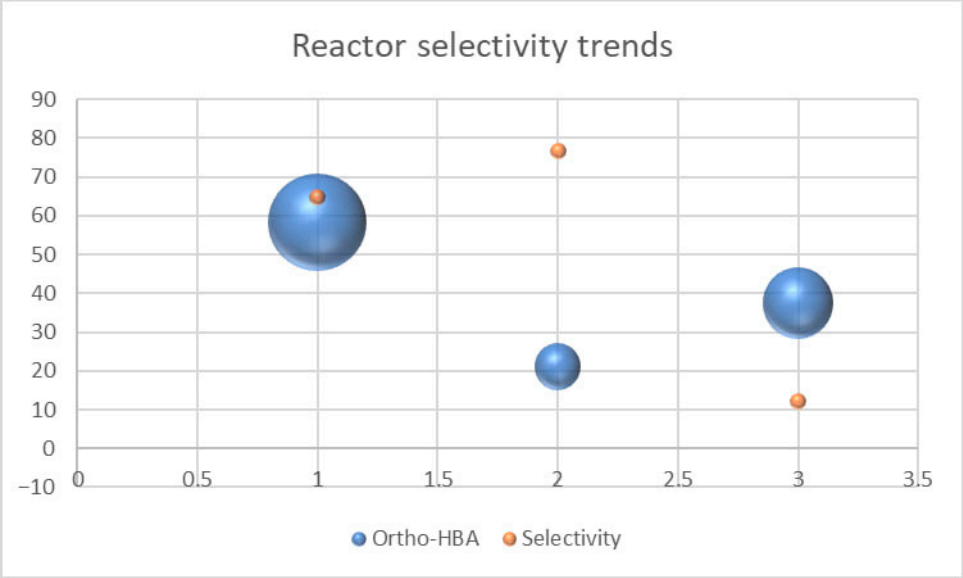

Figure 5. Comparison of the experimental and simulated yields for o-HBA and p-HBA, showing consistent selectivity trends despite absolute yield differences. The deviations (37% for o-HBA, 21% for p-HBA) reflect limitations of the phenomenological yield-based model, which does not capture electrode kinetics or mass transfer effects.

The yields of ortho- and para-hydroxybenzoic acids were measured using high-performance liquid chromatography (HPLC), and the identity of the products was confirmed using gas chromatography-mass spectrometry (GC-MS). The concentration of unreacted NaOH was determined via potentiometric titration.

To accurately evaluate the yield and selectivity of ortho- and para-hydroxybenzoic acids, both experimental results and simulation outputs from Aspen Plus were analyzed. The simulation included key process blocks such as RYield (reaction yield model), Flash separators, and a crystallization stage (Split block), enabling the prediction of product formation and recovery. The experimental data showed higher yields than the simulation due to the presence of electrochemical effects and intermediate stabilization not fully captured by the model.

All laboratory procedures were conducted in accordance with standard safety protocols. CO_2 gas was handled within a ventilated fume hood to avoid inhalation hazards, and personal protective equipment (PPE) was worn throughout all experiments.

The observed discrepancy between the simulated and experimental yields stems from the simplified assumptions inherent to yield-based reactor models in Aspen Plus, which cannot fully replicate electron transfer dynamics, double-layer effects, and catalytic surface phenomena that occur during real electrolysis. Experimental systems also benefit from local temperature gradients and concentration polarization effects that enhance CO_2 activation, while simulations treat the system as perfectly mixed. Future refinements

should include electrochemical kinetic sub-models, potential-dependent rate constants, and surface coverage parameters to more accurately capture the reaction behavior and improve predictive capability.

Faradaic efficiency as a function of applied potential for o-HBA and p-HBA. Maximum FE values of 76.2% (o-HBA) and 66.8% (p-HBA) were achieved at −1.2 V vs. Ag/AgCl. Error bars indicate standard deviation from triplicate measurements (n = 3) in Figure 6.

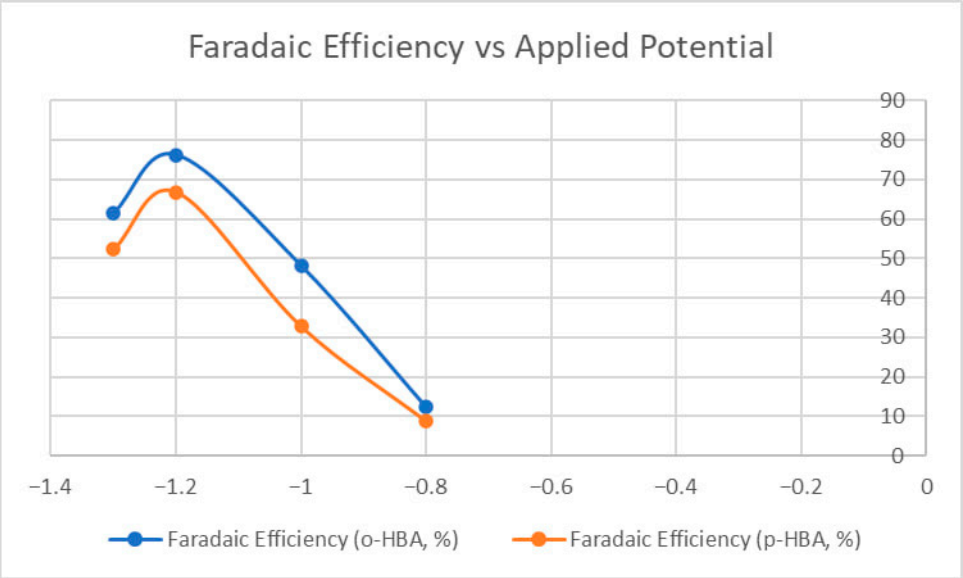

Figure 6. Faradaic efficiency as a function of applied potential for o-HBA and p-HBA.

Overall, the electrochemical synthesis of the ortho- and para-hydroxybenzoic acids in the presence of CO_2 was successfully optimized by integrating experimental data with process simulation. This combined methodology enabled the precise control over process conditions and offered a reliable framework for scaling up sustainable production with improved resource efficiency.

5. Conclusions

The electrochemical synthesis of ortho- and para-hydroxybenzoic acids (o-HBA and p-HBA) from CO_2 was effectively studied and optimized through a combined approach of laboratory experimentation and Aspen Plus process simulation.

This study confirms that electrochemical CO_2 carboxylation offers a sustainable route for producing value-added aromatic compounds, contributing to circular carbon utilization and greener chemical manufacturing. The results provide a mechanistic and quantitative foundation for guiding future scale-up studies of the electrochemical synthesis of hydroxybenzoic acids, offering guidance for future work in optimizing electrode design, reaction kinetics, and industrial-scale process implementation. Integrating experimental data with process simulation ensures both high efficiency and environmentally responsible operation, positioning this approach as a promising strategy in green chemistry.

Supplementary Materials: The following supporting information can be downloaded at: https://www.mdpi.com/article/10.3390/engproc2025117063/s1, Simulation of the process along with parameters.

Author Contributions: Conceptualization, B.E. and R.J.; writing—original draft preparation, B.E. and R.J.; visualization, B.E. and R.J.; writing—review and editing, R.J. and B.E.; supervision, R.J. and B.E. All authors have read and agreed to the published version of the manuscript.

Funding: This research was funded by the Agency of Innovative Development under the Ministry of Higher Education, Science and Innovation of the Republic of Uzbekistan (Contract No. 65).

Institutional Review Board Statement: Not applicable.

Informed Consent Statement: Not applicable.

Data Availability Statement: The raw data supporting the conclusions of this article will be made available by the authors on request.

Conflicts of Interest: The authors declare no conflicts of interest.

References

1. Al Moinee, A.; Rownaghi, A.A.; Rezaei, F. Process Development and Techno-Economic Analysis for Combined and Separated CO_2 Capture-Electrochemical Utilization. *Chem. Eng. J.* **2024**, *499*, 155909. [CrossRef]
2. Alper, E.; Yuksel Orhan, O. CO_2 utilization: Developments in conversion processes. *Petroleum* **2017**, *3*, 109–126. [CrossRef]
3. An, X.; Wang, P.; Ma, X.; Du, X.; Hao, X.; Yang, Z.; Guan, G. Application of ionic liquids in CO_2 capture and electrochemical reduction: A review. *Carbon Resour. Convers.* **2023**, *6*, 85–97. [CrossRef]
4. Banu, A.; Mir, N.; Ewis, D.; El-Naas, M.H.; Amhamed, A.I.; Bicer, Y. Formic acid production through electrochemical reduction of CO_2: A life cycle assessment. *Energy Convers. Manag. X* **2023**, *20*, 100441. [CrossRef]
5. Chen, K.; Fan, Y.; Cao, X.; Liu, J.; Tian, H.; Tian, J. A novel green enzymatic synthetic route of 2, 3-dihydroxybenzoic acid from glucose and CO_2 fixation. *Process Biochem.* **2020**, *94*, 207–212. [CrossRef]
6. Chen, T.; Wang, C.; Cheng, L.; Zhang, J. Carbon dioxide resource utilization in methanol products: Carbon emission projections, visual analysis, life cycle assessment. *J. Indian Chem. Soc.* **2024**, *101*, 101336. [CrossRef]
7. Fan, Z.; Wang, X. Study of the proton transfer during acidification of sodium salicylate based on ReaxFF molecular dynamics simulation. *J. Mol. Liq.* **2024**, *414*, 126213. [CrossRef]
8. Fu, L.; Qu, Z.; Zhou, L.; Ding, Y. Boosting electrochemical CO_2 reduction to CO over interfacial hydroxide-metal catalysts. *Appl. Catal. B Environ.* **2023**, *339*, 123170. [CrossRef]
9. Gollapudi, D.; Eswaraditya Reddy, L.; Mahnot Jain, G.; Kolluru, S.; Ramesh, G.V. Advanced copper-based electrocatalysts for the electrochemical reduction of carbon dioxide to valuable fuels: Recent advances. *Mater. Today Proc.* **2024**. [CrossRef]
10. Gulzar, A.; Gulzar, A.; Ansari, M.B.; He, F.; Gai, S.; Yang, P. Carbon dioxide utilization: A paradigm shift with CO_2 economy. *Chem. Eng. J. Adv.* **2020**, *3*, 100013. [CrossRef]
11. Li, Y.; Wang, H.; Yu, Y.; Zhang, Z. 4E evaluation and multi-objective optimization of low concentration flue gas CO_2 capture and multi-product conversion process. *Sep. Purif. Technol.* **2025**, *359*, 130625. [CrossRef]
12. Liang, S.; Altaf, N.; Huang, L.; Gao, Y.; Wang, Q. Electrolytic cell design for electrochemical CO_2 reduction. *J. CO_2 Util.* **2020**, *35*, 90–105. [CrossRef]
13. Matthessen, R.; Fransaer, J.; Binnemans, K.; De Vos, D.E. Electrocarboxylation: Towards sustainable and efficient synthesis of valuable carboxylic acids. *Beilstein J. Org. Chem.* **2014**, *10*, 2484–2500. [CrossRef]
14. Orlić, M.; Hochenauer, C.; Nagpal, R.; Subotić, V. Electrochemical reduction of CO_2: A roadmap to formic and acetic acid synthesis for efficient hydrogen storage. *Energy Convers. Manag.* **2024**, *314*, 118601. [CrossRef]
15. Sabia, G.; Heinze, C.; Alobaid, F.; Martelli, E.; Epple, B. ASPEN dynamics simulation for combined cycle power plant—Validation with hot start-up measurement. *Energy* **2019**, *187*, 115897. [CrossRef]
16. Sarmad, S.; Lu, D.; Gao, S.; Sun, Z.; Zhou, Z.; Ali, A.; Duan, L. Advancing syngas production: A comparative techno-economic analysis of ICCU and CCU technologies for CO_2 emission reduction. *J. Environ. Chem. Eng.* **2024**, *12*, 114562. [CrossRef]
17. Shanthi, B.; Palanivelu, K. Conversion of carbon dioxide to resorcylic acid under ultrasonication by Kolbe–Schmitt reaction. *Ultrason. Sonochem.* **2015**, *27*, 268–276. [CrossRef]
18. Singh, S.; Patidar, R.; Srivastava, V.C.; Lo, S.-L.; Nidheesh, P.V. A critical review on the degradation mechanism of textile effluent during electrocatalytic oxidation: Removal optimization and degradation pathways. *J. Environ. Chem. Eng.* **2023**, *11*, 111277. [CrossRef]
19. Su, W.; Jiang, Y.; Zuo, X.; Li, C.; Wang, H. Engineering nucleation/crystallization to intensify the enzymatic reactions and fermentation: A review. *Chem. Eng. J.* **2022**, *431*, 134186. [CrossRef]
20. Van Daele, S.; Hintjens, L.; Hoekx, S.; Bohlen, B.; Neukermans, S.; Daems, N.; Hereijgers, J.; Breugelmans, T. How flue gas impurities affect the electrochemical reduction of CO_2 to CO and formate. *Appl. Catal. B Environ.* **2024**, *341*, 123345. [CrossRef]
21. Yang, X.; Xu, L.; Zhu, Y.; Zhang, S.; Jia, G.; Du, J. Efficient fabrication of oxazolidinones for the carboxylative cyclization with carbon dioxide. *J. CO_2 Util.* **2023**, *74*, 102531. [CrossRef]
22. Zaman, A.C. Hydroxybenzoic acid derived porous carbons for low pressure CO_2 capture. *J. Solid State Chem.* **2023**, *327*, 124245. [CrossRef]

23. Zhang, H.; Zhang, J.; Jiang, W.; Mu, X.; Tang, Y.; Duan, Z. Molecular dynamics simulation of the Kolbe-Schmitt carboxylation mechanism of sodium phenoxide. *Chem. Eng. Sci.* **2024**, *286*, 119690. [CrossRef]
24. Zhang, X.-B.; Liu, Y.-X.; Luo, Z.-H. Kinetic study of the aqueous Kolbe-Schmitt synthesis of 2,4- and 2,6-dihydroxybenzoic acids. *Chem. Eng. Sci.* **2019**, *195*, 107–119. [CrossRef]
25. Eshqulov, B. *Electrochemical Synthesis of Ortho- and Para-Hydroxybenzoic Acids Using CO_2: Experimental and Simulation-Based Optimization*; Zenodo: Geneva, Switzerland, 2026; Supplementary data: Aspen Plus simulation. [CrossRef]

Disclaimer/Publisher's Note: The statements, opinions and data contained in all publications are solely those of the individual author(s) and contributor(s) and not of MDPI and/or the editor(s). MDPI and/or the editor(s) disclaim responsibility for any injury to people or property resulting from any ideas, methods, instructions or products referred to in the content.